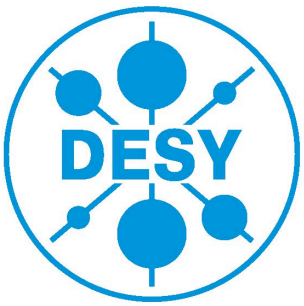

TCT - Measurements and Software Development

Mykyta Haranko, Taras Shevchenko National University of Kyiv, Ukraine

mykyta.haranko@gmail.com

September 9, 2015

Abstract

A sequence of measurements of un-irradiated silicon sensors using the Transient Current Technique (TCT) performed. Operation of the red (640 nm) and infrared (1060 nm) lasers with different configurations were studied. A new universal sensor mount and the PCB designed at DESY for Top-, Edge- and Bottom- TCT were tested. Data analysis framework developed by Hendrik Jansen was extended and is presented in this report.

Contents

1 Introduction

Silicon is one of the most studied materials, it's used widely in industry and physics. Nowadays the majority of tracking and vertex detectors are made of silicon, for example, experiments such as ATLAS, CMS, where particles are created due to the proton-proton collisions. At the High Luminosity phase of the LHC (HL-LHC) inner sensors are expected to integrate a fluence of about 10^{16} n_{eq}/cm^2. The main task is to design a completely new detectors with high radiation hardness. One of the most important characteristics is the signal after irradiation: it decreases due to low trapping times of the charge carriers in the irradiated materials. In Figure 1 simulations [1] of the electric field distribution before and after irradiation is shown for a 200 μm pixel sensor. For

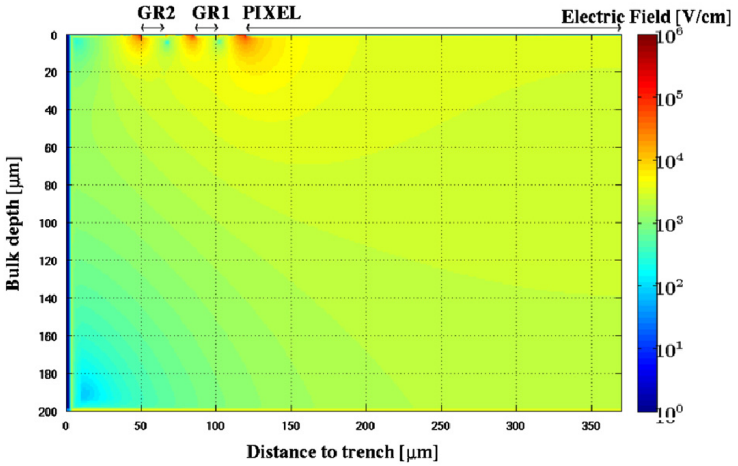

(a) Non-irradiated device

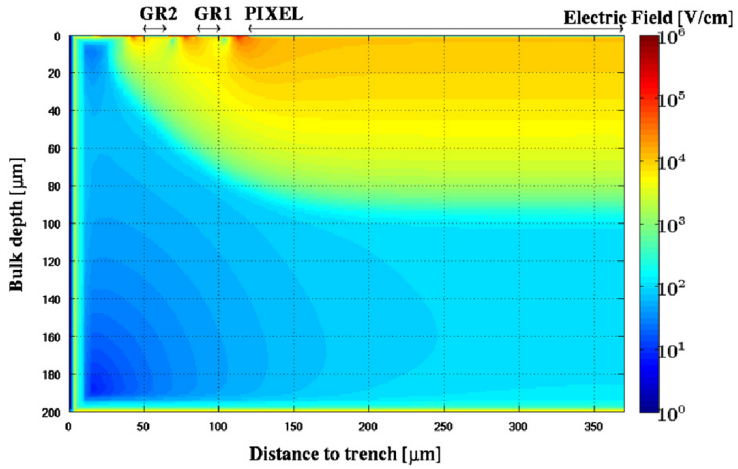

(b) Device irradiated with a fluence 10^{15} n_{eq}/cm^2

Figure 1: Simulation of the electric field distribution of the 200 μm pixel sensor at the 50 V bias voltage.[1]

the same bias voltages (50V) the irradiated sensor is undepleted. Each detector has to

be studied after irradiation before using it at the high-energy physics experiment.

The Transient Current Technique (TCT) is widely used for studying the detector response after high irradiation fluences. The main idea is to use laser to produce charge carriers in the sensor, which is similar to the energy loss process of a minimum ionizing particle crossing the detector.

2 Experimental Setup

In Figure 2 a schematic view of the experimental setup is shown. At first a sample

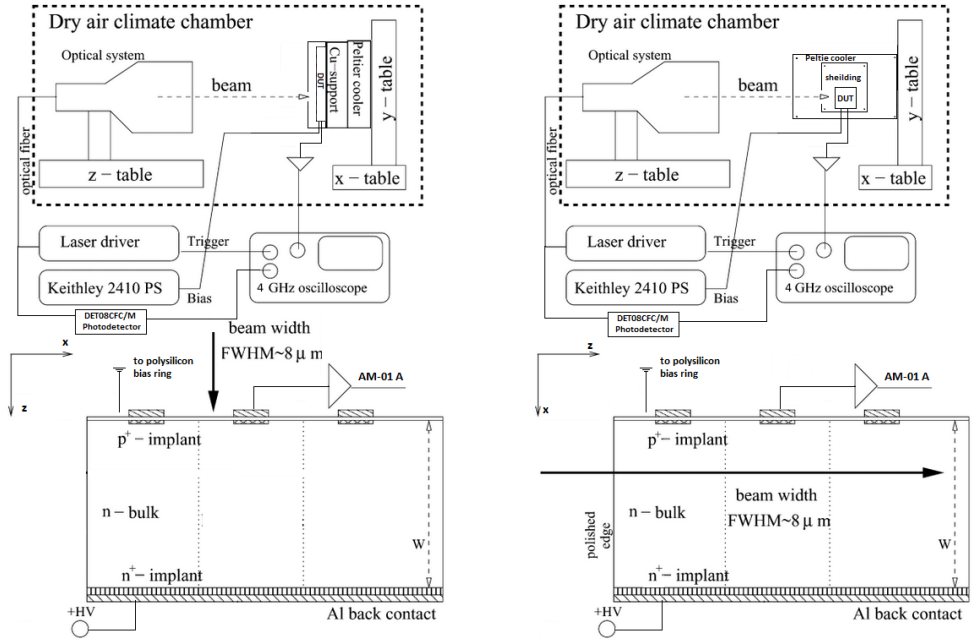

(a) Top-TCT Configuration (b) Edge-TCT Configuration

Figure 2: Schematic view of the experimental setup.[2]

sensor from Particulars was connected to a high voltage supply (Keithley 2410) through a bias-T. This configuration is not shown. Top-TCT measurements were done for this sample. Secondly, the new mount and PCB were used, in this configuration ground was connected to the bias ring, backside of the sensor was connected to the high voltage line and two of the AC-coupled readout strips close to the edge were directly connected to the wide band amplifiers (Particulars AM-01 A), see Figure 2. Amplifiers were connected to a power supply. The induced current pulses were digitized and stored using the LeCroy 640Zi 4GHz Oscilloscope. The second configuration can be used for both edge- and top-TCT measurements, as shown in Figure 2.

After laser pulse shot onto the detector edge or top side (that is the difference between edge- and top- TCT), electron-hole pairs are created in the bulk. Charges start to drift in the electric field. The electrical current is observed on the strips. In Figure 3 the creation of the charges during the Edge-TCT measurements is shown schematically.

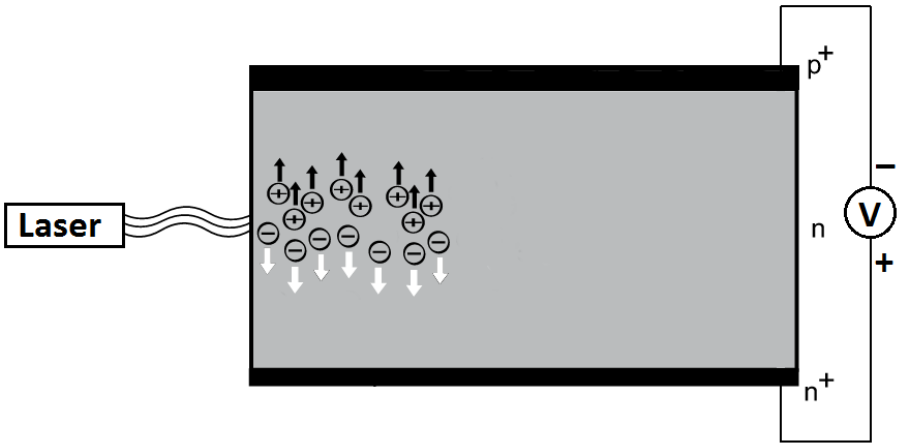

Figure 3: Schematic view of the charge creation process, Edge-TCT.

3 Lasers

Two lasers produced by Particulars were used to create free electron-hole pairs in the sensor: an infra-red (1060 nm) fibre-coupled laser (LA-01 IR (FC)) and a red (640 nm) fibre-coupled laser (LA-01 R (FC)). The time stability and the amount of light deviation were measured. Also the response of the photodetectors DET08CFC/M (InGaAs, 800 nm -1700 nm), DET025AFC/M (Si, 400 nm -1100 nm) was studied. Light from the lasers transports through the fibers, passing the lightsplitter, which splits the light with fraction 10% to 90%. Successfully, 90% of the light aimed to the sensor and the 10% aimed to the photodetector, see Figure 4.

Figure 4: Schematic view of the light splitter.

3.1 Red Laser

The red laser produces the light of the 640 nm wavelength. A typical signal from the photodetector is shown in Figure 5. The charge in arbitrary units is extracted by integrating the signal in a fixed time range, which is shown with black lines in Figure 5.

One of the most important problems for the red laser - high power decreasement in time, what is shown in Figure 6: laser power decreases by factor of 2 during the first two hours of operation. Later the power still decreases but with smaller slope.

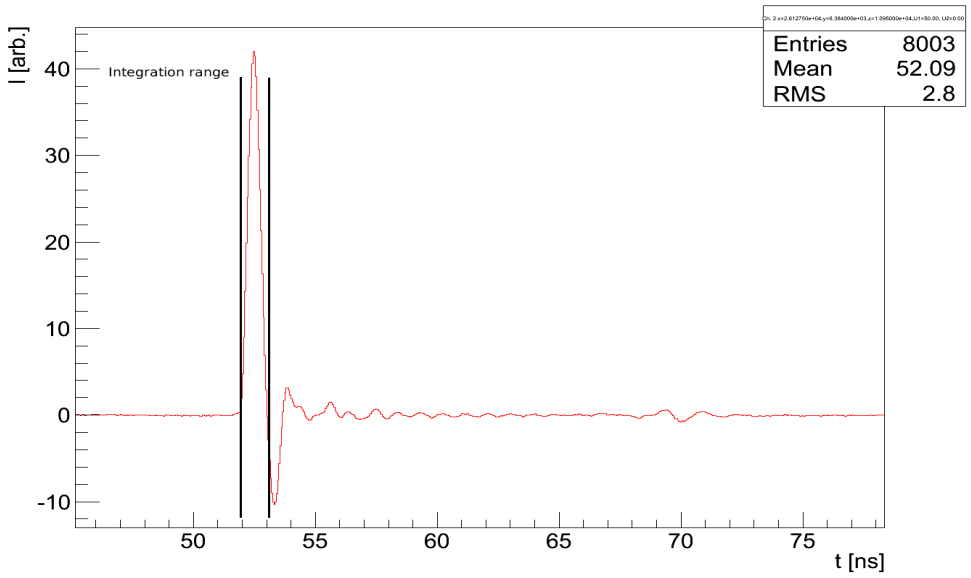

Figure 5: Signal from the photodetector, red laser (640 nm). Averaged over 50 waveforms.

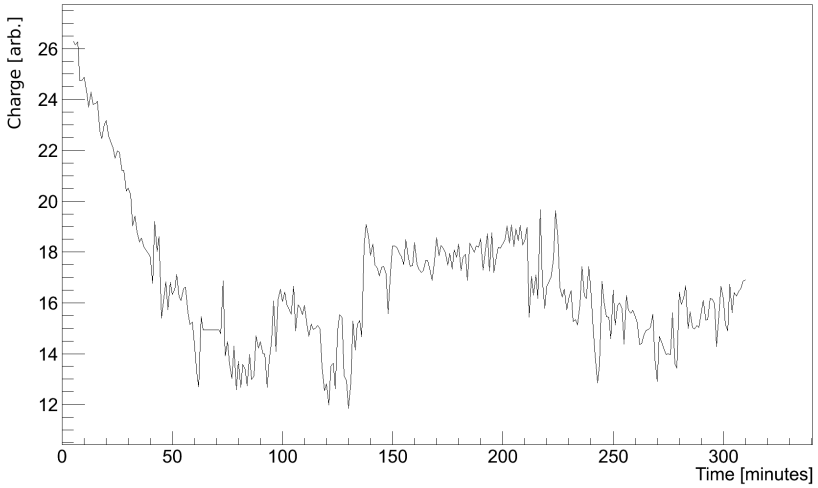

Figure 6: Red laser charge vs time, each point averaged over 100 waveforms.

The RMS of the measured charge in the small time range (less than 2 minutes) was taken at the beginning of the operation and after 5.7 hours, see Figure 7. The RMS is still 30% even after stabilization, the data has to be normalized by the amount of light measured using the photodetector.

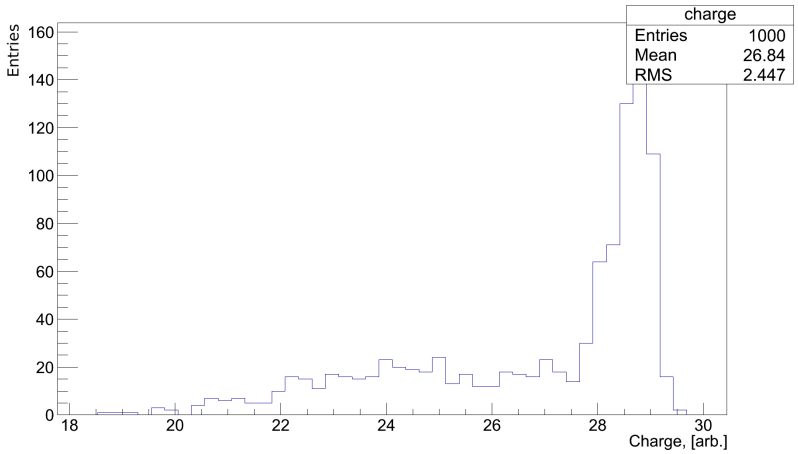

(a) Beginning of the operation (3 minutes)

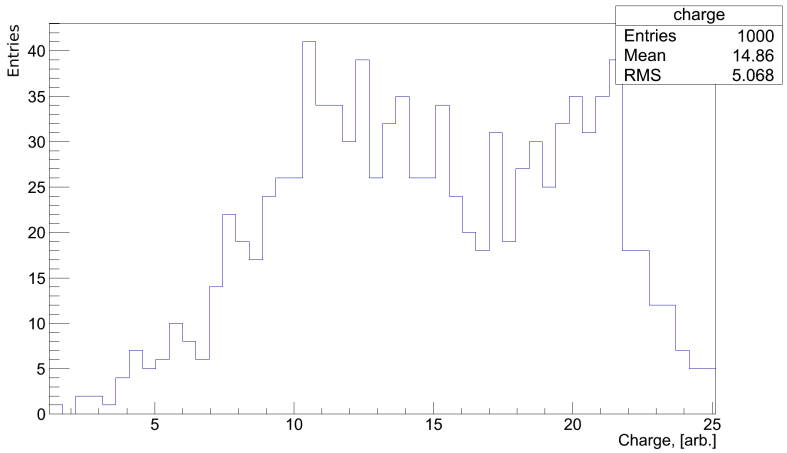

(b) After stabilization (5.7 hours)

Figure 7: Red laser power deviation measured in a small time window.

3.2 Infra-red Laser

The infrared laser produces light of the 1060 nm wavelength. A typical signal from the photodetector is shown in Figure 8. The charge in arbitrary units is extracted by integrating the signal in a fixed time range, which is shown with black lines in Figure 8.

The power decreasement of the infra-red laser even at the beginning of operation is small - power drops only by 3% during the first two hours of operation. The same is for the RMS: after 2.2 hours of operation infra-red laser shows the deviation of 0.5% (See Figure 10) comparing to 1% (not shown) at the beginning of operation.

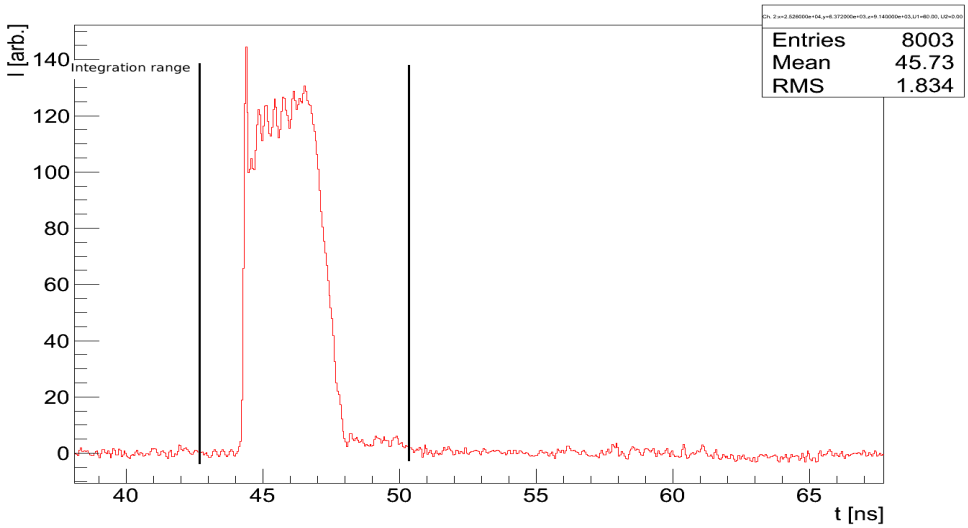

Figure 8: Signal from the photodetector, infra-red laser (1060 nm). Averaged over 50 waveforms.

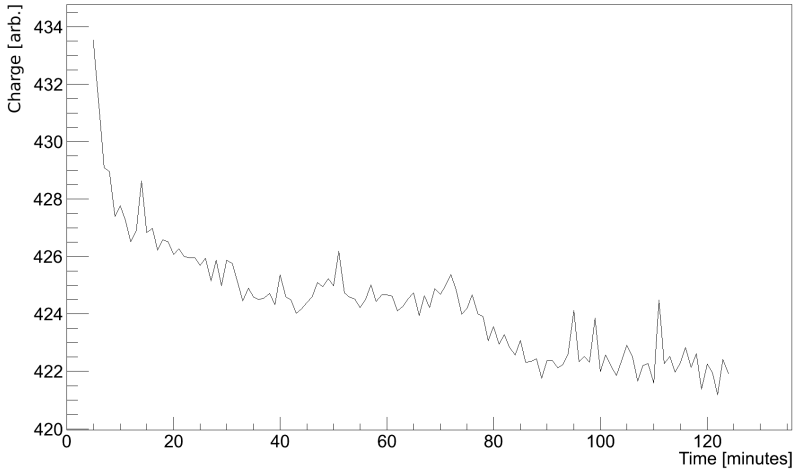

Figure 9: Infra-red laser power vs time, each point averaged over 100 waveforms.

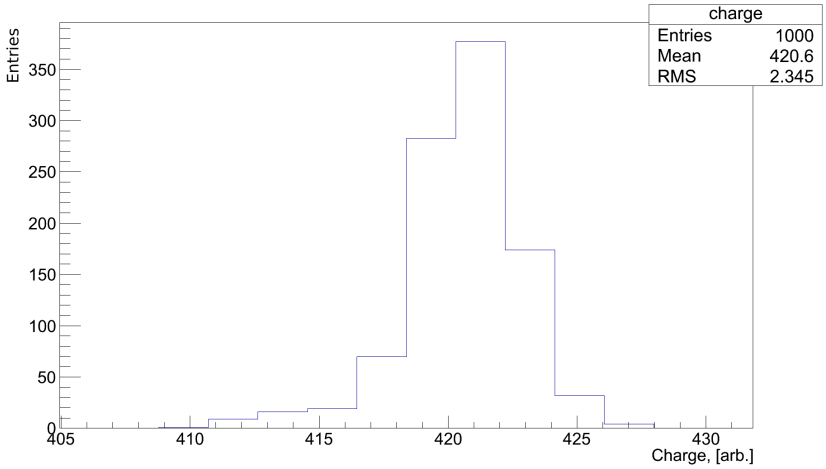

Figure 10: Infra-red laser power deviation measured in a small time window after 2.2 hours of operation.

For both lasers power decreasement in time was observed, what means that photodetectors have to be used to normalize the data in time. Also the red laser has very high power RMS, even for the averaged signal, see Figure 7.

4 Top-TCT

As it was shown in Figure 2(a), Top-TCT is defined by illuminating of the sensor top surface. Top-TCT is used to extract such quantities as the depletion voltage, velocity of the charge carriers, which is used for calculation of the mobilities of electrons and holes.

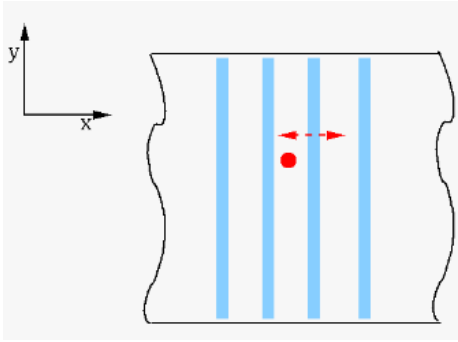

(a) Scan along X axis.

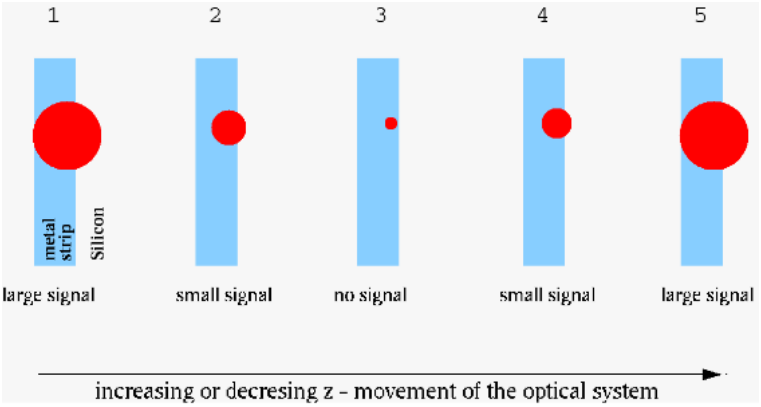

(b) Changing of the beam spot size due to the different optical distances.

Figure 11: Schematic representation of the focus search method for a strip detector.[4]

4.1 Focus Search

The first step is the focus search. To find the focus for a strip sensor one need to follow instructions proposed in Ref.[4]. The basic idea is shown in Figure 11(a): when moving the beam spot along the X axis, less charge will be observed at the strip region - part of light will be reflected from the strip. Then, by changing the optical distance,

the size of the beam spot can be changed (Figure 11(b)). In Figure 12 the curves for focused and un-focused beam are shown. If the beam is out of focus, charge measured using the sensor, starts to increase slowly when scanning along the X-axis. This curve could be fitted using the error function, and the FWHM value can be extracted from the fit. When the beam spot gets smaller, the same happens to the FWHM value.

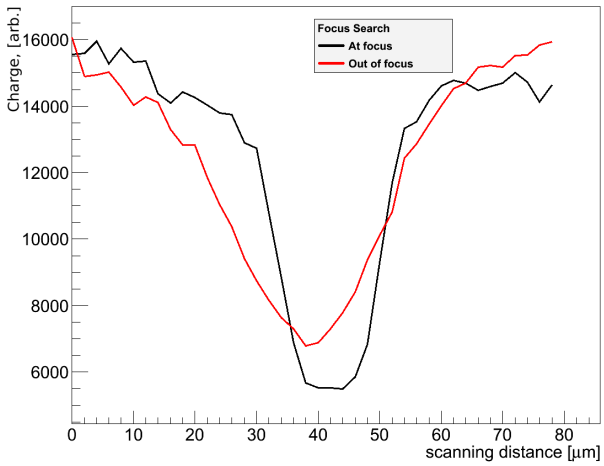

Figure 12: Scans for focused and un-focused beam, Top-TCT.

The FWHM is plotted for different optical distances and fitted with the second-order polynomial, see Figure 13. The position with the smallest value of the FWHM is defined to be a focus position.

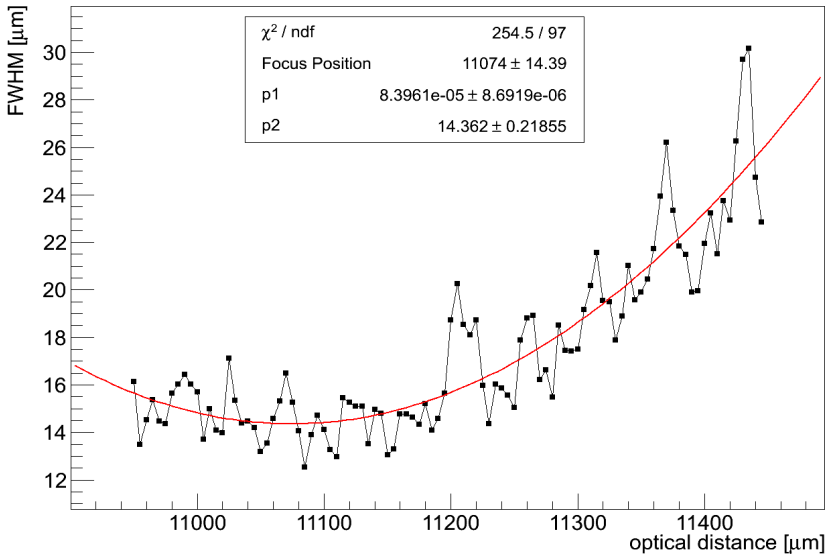

Figure 13: FWHM values for different optical positions, Top-TCT.

4.2 Depletion Voltage

To find the depletion voltage, the charge collected at certain position between strips for the different bias voltages has to be integrated. After reaching the depletion voltage charge stops to increase and becomes constant. Plotting the charge with square root of voltage, the dependency can be obtained, which has to be fitted with two lines - one fits the rising part, second one - the constant part, when all charge is collected (detector is fully depleted). The intersection of these curves gives the value of the full depletion voltage. For the sample sensor from Particulars Figure 14 shows the depletion voltage value of 33.6 V.

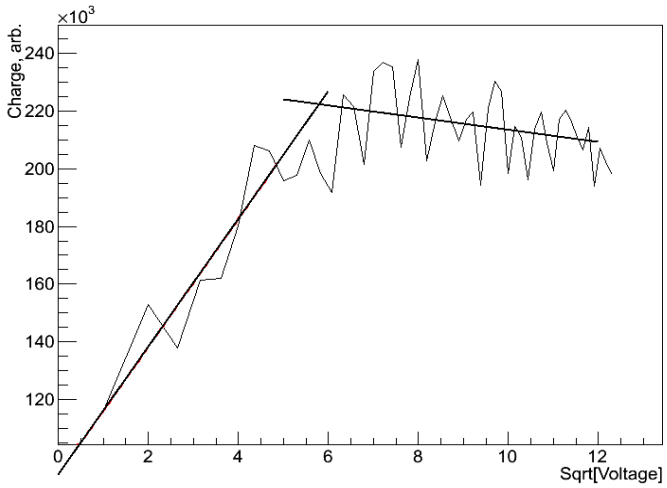

Figure 14: Depletion voltage search, Top-TCT.

4.3 Mobility

The TCT is used to calculate the charge carrier mobility. The 80% of the red light is absorbed after 5 μm of silicon[5] - this is used to measure the charge carrier mobility of different type. After applying positive voltage to the strips (p-type bulk sensor from Particulars) and negative to the back side, holes drifting to the back side and electrons to the strips. Shooting from the top side: electrons are collected immediately, and the transit time is the time of the hole drift.

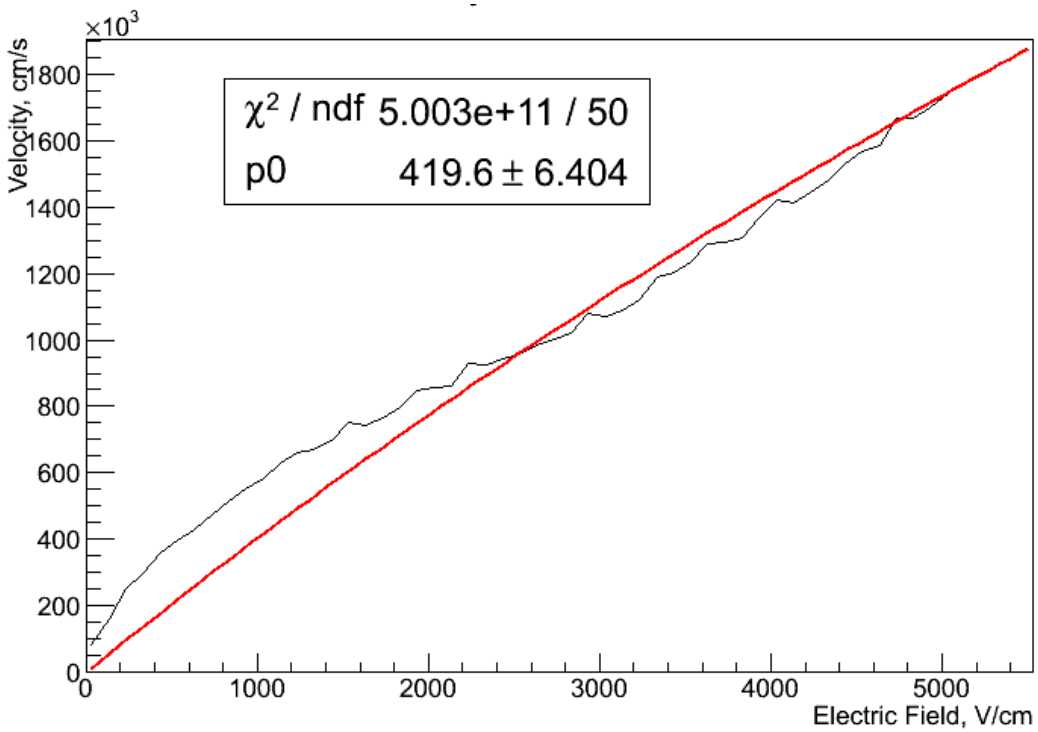

Figure 15: The average hole drift velocity for p-type sensor from Particulars.

The average hole drift velocity through the sensor is given by $v_h = \frac{W}{t_{transit}}$, where $t_{transit}$ is the duration of the signal, W is the thickness of the sensor. For the sample sensor from Particulars the average hole drift velocity is shown in Figure 15. The fit function is given by (1), according to the (2), where v_{sat} is the holes saturation velocity, μ_0 is the low-field mobility, E is the electric field. The fit results in a value of $419.6 \frac{cm^2}{Vs}$, with assumption of detector thickness 300 μm and saturation velocity in silicon of $v_{sat} = 1 \times 10^7 \frac{cm}{s}$.

$$f(E) = \frac{p_0 E}{1 + \frac{p_0 E}{v_{sat}}}. \tag{1}$$

$$v_h(E) = \frac{\mu_0 E}{1 + \frac{\mu_0 E}{v_{sat}}}. \tag{2}$$

5 Edge-TCT

As it was shown in Figure 2(b) and explained further, laser light is directed perpendicularly to the edge of the detector.

5.1 Sensor Preparation

After cutting the sensor (CE2339, [6]) from waver with diamond cut, surface is highly damaged. In Figure 16(a) high reflection of the light from the surface can be observed.

This caused by the scratches on top of the surface, therefore it requires polishing. First sample was polished using a 0.3 μm diamond polishing paste mixed with water. The result is shown in Figure 16(b).

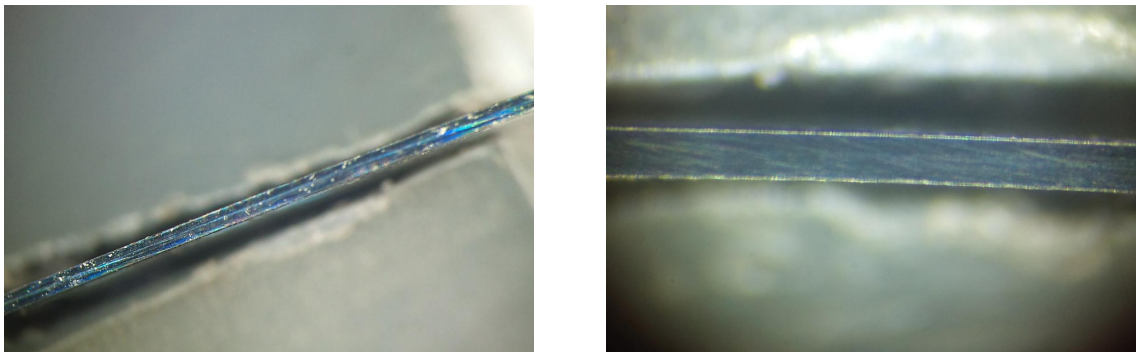

(a) The edge before polishing (b) The edge after polishing

Figure 16: Photos of a sensor edge under a microscope.

After polishing the sensor was bonded to the PCB designed at DESY. Two strips were bonded - 4th and 5th from the edge. Bias voltage is applying from the back side through the bias pad. Bias ring connected to the ground setting the zero potential to the strips through the polysilicon resistors, see Figure 17.

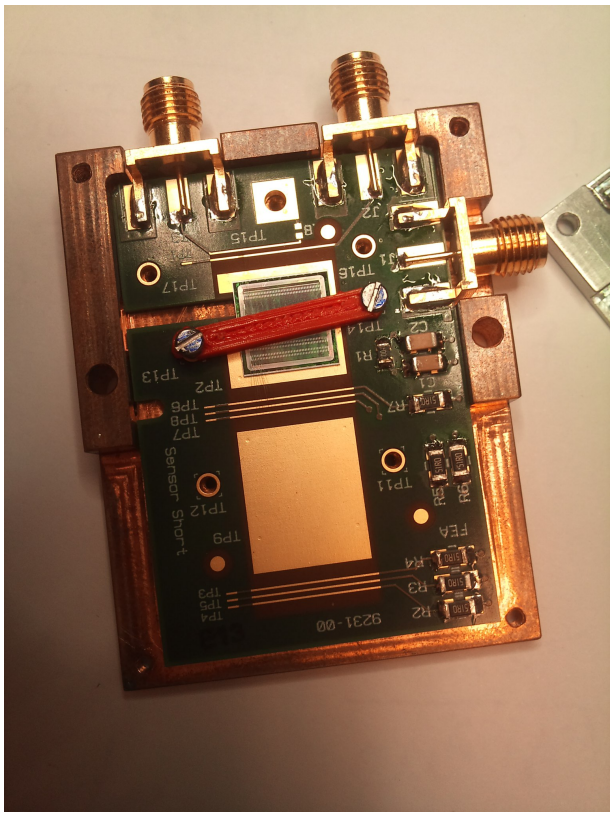

Figure 17: The sample sensor CE2339 bonded to the PCB with copper mount.

5.2 Leakage Current

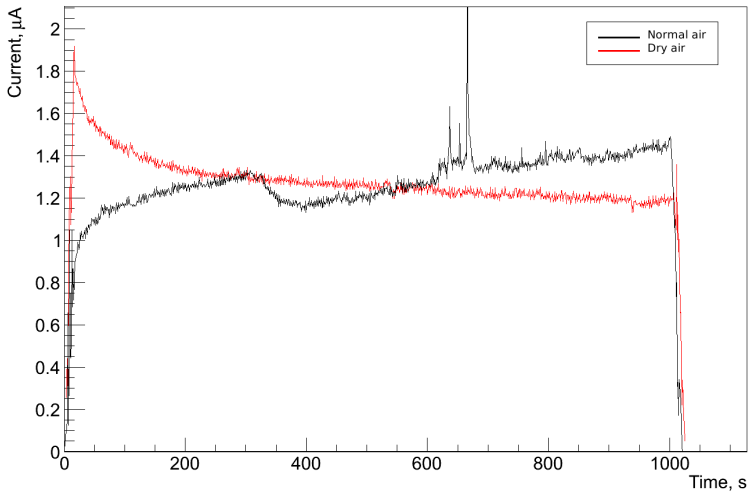

Figure 18: Leakage current of the test sensor CE2339 as a function of time in different conditions, $U_{bias} = 90$ V.

An important characteristic of the test sample is its leakage current, which is dominated by thermally generated electron-hole pairs. Due to the applied electric field they cannot recombine and are separated. The drift of the electrons and holes to the electrodes induces the leakage current. Also the surface current going through the edge of the detector adds some part to the total leakage current. For the test sample (bias voltage - 90 V) the leakage current as a function of time is presented in Figure 18. The part before 300 seconds differs due to the different starting conditions, but the following data shows several small breakdowns for normal conditions, which could be explained by the presence of dust and water molecules.

5.3 Alignment

For the Edge-TCT measurements the test sample needs to be aligned. In Figure 19 charge profiles for for aligned and misaligned sensor are shown. The misalignment appears as the different thickness of the detector, which should be constant (280 μm for CE2339 sample). The amplitude is smaller due to the fact, that less light absorbed when sample is misaligned.

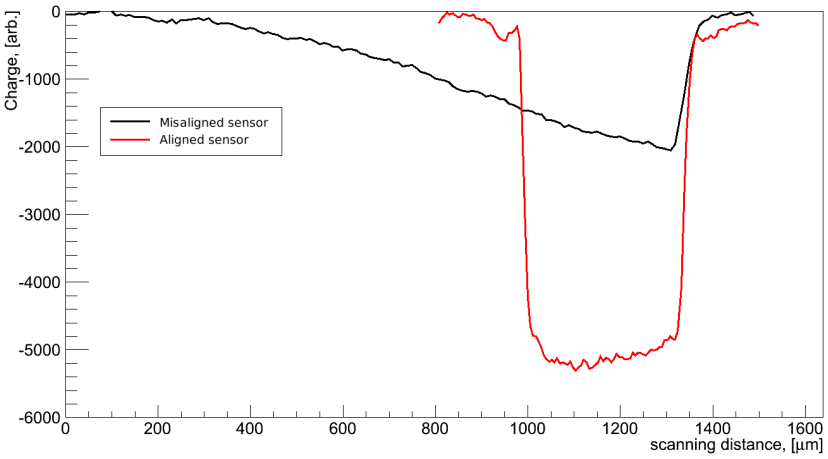

Figure 19: Edge-TCT scan for aligned and misaligned sensor. Sensor thickness is 280 μm.

5.4 Focus Search

To find the focus with Edge-TCT the same approach is used as for the Top-TCT measurements. Instead of scanning and passing the strips, scan is done along the entire detector thickness. The charge profile falling and rising edge are fitted, as it is shown in Figure 20(a). Red arrow shows the direction of the scan. FWHM values are taken from the fits and plotted for different optical distances, then fitted as it shown in Figure 20(b).

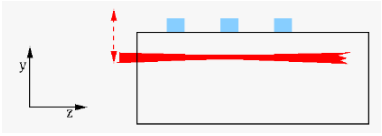

(a) Schematics

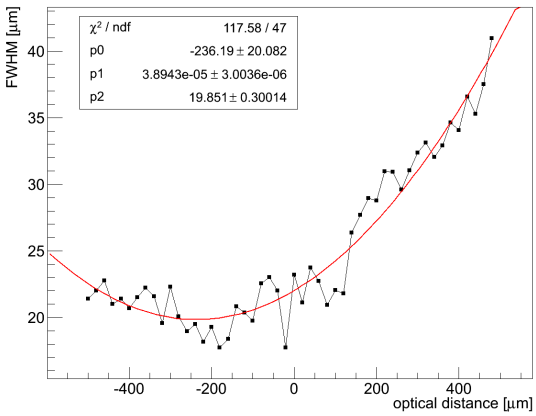

(b) FWHM as a function of optical distance, Edge-TCT.

Figure 20: Edge-TCT laser beam focusing.

5.5 Depletion Voltage

The charge profiles for different bias voltages in arbitrary units are shown in Figure 21. When the detector is not fully depleted the signal near the bottom of the detector still can be observed due to the different doping concentrations in the n and n+ layers.

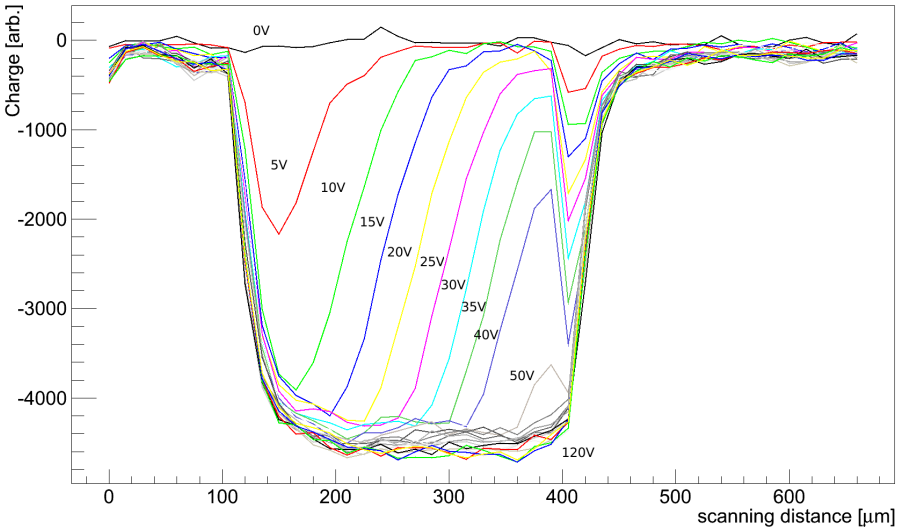

Figure 21: Charge profiles for different voltages, Edge-TCT.

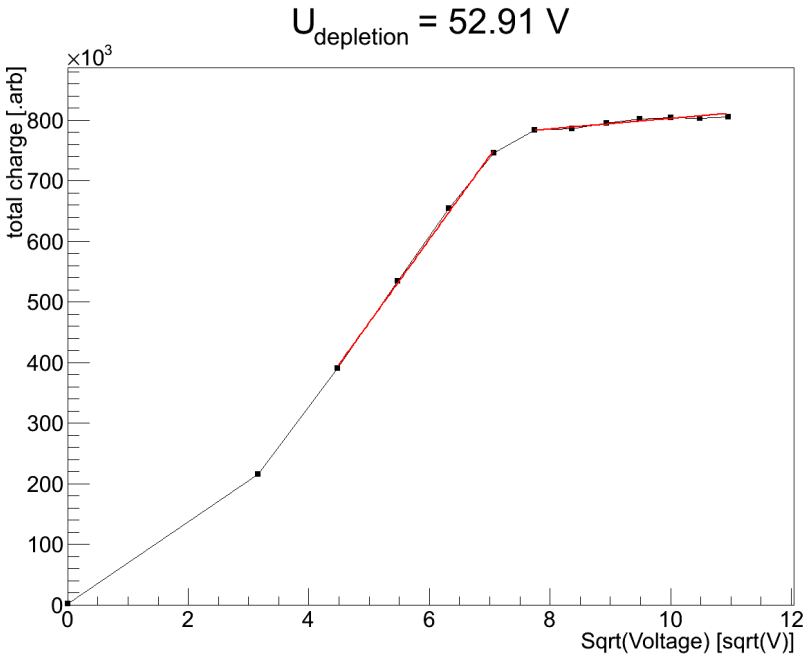

Figure 22: Depletion voltage of the CE2339 sample sensor.

Depletion voltage was found using the same method, as it was used for the Top-TCT measurements, see Section 4.2, but the charge is also integrated through all the detector thickness. As it shown in Figure 22, obtained value is 52.91 V and is consistent with the value of 49 V measured using the probe method.

5.6 Electric Field Profiles

The induced current in the detector can be expressed by (3), where e_0 is the elementary charge, $N_{e,h}$ is the number of created e-h pairs near the strip, A is the amplifier amplification, $\tau_{eff,e,h}$ is the effective trapping time, $v_{e,h}$ is the drift velocity and E_ω is the weighting field. For simple pad detectors term $\overrightarrow{v}_{e,h}(t) \cdot \overrightarrow{E}_\omega$ is simply $\frac{v_{e,h}}{W}$, where W is the detector thickness.

$$I_{e,h}(t) = Ae_0 N_{e,h} \exp(-\frac{t}{\tau_{eff,e,h}}) \overrightarrow{v}_{e,h}(t) \cdot \overrightarrow{E}_\omega. \tag{3}$$

According to the Ref. [2], Prompt Current Method is used to obtain the electric field profiles. The measured current amplitude immediately after charge carrier generation ($\exp(-\frac{t}{\tau_{eff,e,h}}) \approx 1$) can be expressed as:

$$I(y, t \sim 0) = Ae_0 N_{e,h} \frac{v_e(y) + v_h(y)}{W} = Ae_0 N_{e,h} \frac{\mu_e(y) + \mu_h(y)}{W} E(y). \tag{4}$$

From this point there could be two ways: one way to extract the electric field profiles is to use the estimation of the charge carriers number from the laser power, measured using the photodetector. But the problem is that one need precise values of the amplification, $N_{e,h}$ - which is difficult to estimate due to the loses in the optical system, in the silicon, etc. The second way is to use formula (5) as the constraint and to solve numerically the equation (4). That was done using the bisection method[7].

$$V_{bias} = \int_0^W E(y) dy. \tag{5}$$

As the result the electric field profiles were extracted and are presented In Figure 23.

Also the velocity profiles could be extracted using equation (6), where v_{sat} is the holes saturation velocity, μ_0 is the low-field mobility, E is the electric field.

$$v_h(E) = \frac{\mu_0 E}{1 + \frac{\mu_0 E}{v_{sat}}}. \tag{6}$$

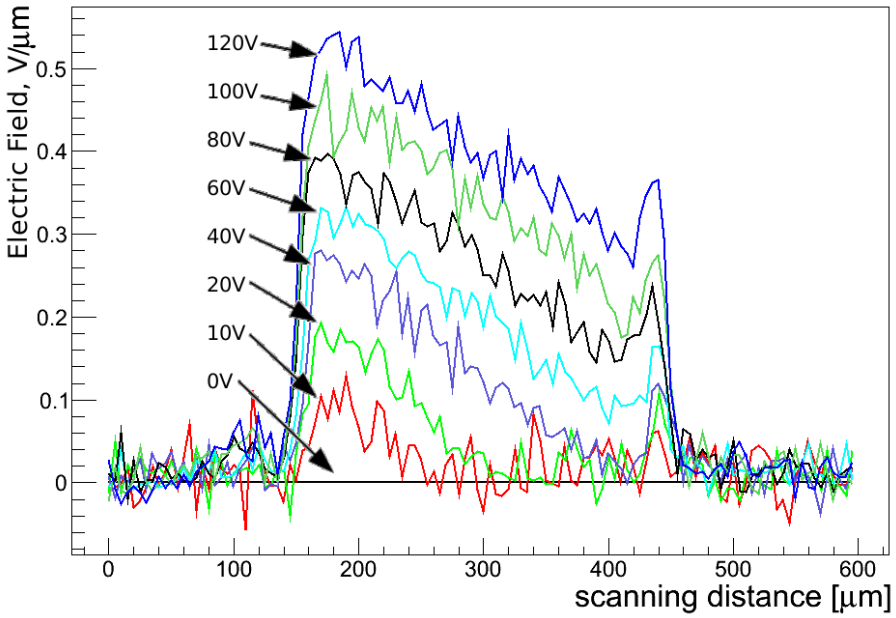

Figure 23: Field profiles for different voltages, Edge-TCT.

6 Software Description

The framework by Hendrik Jansen was extended. Here you can find the description of the new code that was written. To fetch the latest version one should visit the GitHub repository and follow the instructions. The configuration is set in the *.txt file, which is passed by "-af */*.txt" parameter during the framework execution. Configuration file is described in the Table 1.

The new class was implemented to process the data from the PSTCT program, which performs the measurements. This class uses the TCTAnalyse library to read the raw data from the scans. To perform the processing one creates an instance of the class, for example, using *TCT::Scanning daq_data* command. And then runs the *ReadTCT* method of the class, passing the data folder and the instance of the *analysis* class, which contains the configurations. This steps have been already done at the *main.cxx* file of the framework.

The methods of the Scanning class are described in the Table 6. Each method at the beginning checks if all the required data is present in the current scan. If the photodiode data is present, output of the processing also contains the results with normalized data.

Some additional methods were not described here, they are used to build plots, fitting of the functions, etc.

Table 1: Configuration File Description

Parameter	Value	Description
Mode	Setting the acquisition mode	
	0	Taking the sets of single measurements (*.txt or *.raw files by oscilloscope).
	1	Taking the data from *.tct file produced by DAQ software.
LeCroyRAW	Setting the source of the data for single waveform acquisition	
	0	Using the standard method, data is taken from the *.txt files
	1	Using the LeCroyConverter library, data is taken from the *.raw files
Scanning		
CH_Detector	1,2,3,4	Oscilloscope channel of the test sensor
CH_Photodiode		Oscilloscope channel of the photodetector
CH_Trigger		Oscilloscope channel of the trigger
Optical_Axis	1,2,3	Setting the optical axis: 1-x,2-y,3-z
Scanning_Axis	1,2,3	Setting the scanning axis: 1-x,2-y,3-z
VoltageSource	1,2	Setting the voltage source
Movements_dt	s	Time between XYZ stage movements
TCT_Mode	0	Top-TCT Mode
	1	Edge-TCT Mode
	2	Bottom-TCT Mode. NOT IMPLEMENTED YET
Focus_Search	0,1	Turn Off/On the focus search method. Performs operation only for TCT-Mode, that was set
TimeSensorLow	ns	Integrate the sensor signal from TimeSensorLow to TimeSensorHigh
TimeSensorHigh		
TimeDiodeLow	ns	Integrate the photodetector signal from TimeDiodeLow to TimeDiodeHigh
TimeDiodeHigh		
SaveSeparateCharges	0,1	Write charge,velocity,field plots to the separate plots, instead of using only MultiGraph
SaveSeparateWaveforms	0,1	Writes separate waveforms for different positions, voltages.
EdgeDepletionVoltage	0,1	Turn Off/On the Depletion Voltage Search method
EdgeVelocityProfile	0,1	Turn Off/On calculation of the electric field, velocity profiles
EV_Time	ns	Averaging the current in range (TimeSensorLow,TimeSensorLow+EV_Time)

Table 2: Scanning Methods Description

bool Scanning::ReadTCT(char* filename, analysis *ana1, bool HasSubs)
Main method, opens the data file, corrects the base line, creates the output file. Also, if needed saves all the acquired waveforms to the output *.root file. Then, the method steers the analysis according to the configuration.
bool Scanning::CheckData()
Basic check. Checks if the oscilloscope channels that was set at the configuration file contain data.
bool Scanning::CheckFocus()
Checks if data contain at least 10 points along the scanning axis.
bool Scanning::DoTopFocus()
Focusing of the beam using the Top-TCT scan data. Method calculates charges by integrating the current and fits the data. Position of the strip, FWHM, minimum charge, strip thickness, misalignment between the optical and scanning axes are extracted. FWHM and Minimum Charge are fitted by the second order polynomial to find a focus position.
bool Scanning::DoEdgeFocus()
Focusing of the beam using the Edge-TCT scan data. Edges of the detector are fitted, from this data position of the top,bottom sides are extracted. Also FWHM, thickness of the detector calculated. FWHM is fitted by the second order polynomial to find a focus position.
bool Scanning::CheckEdgeDepletion()
Checks if data contain scans for at least 7 different voltages to find the depletion voltage. And also 10 points along the scanning axis.
bool Scanning::DoEdgeDepletion()
Searching for the depletion voltage. Method fits the edges of the detector and then integrates the charge in this ranges for different voltages. Plotting the charge with squared root of the voltage, and fitting the plot with two lines helps find a depletion voltage.
bool Scanning::CheckEdgeVelocity()
Checks if data contain at least 10 points along the scanning axis.
bool Scanning::DoEdgeVelocity()
Method builds the electric field profiles, velocity profiles according to the method described at the Section 5 of this report. Also there is a possibility to find an electric field profiles without the bias voltage integral constraint - but this part is not finished for the moment.

bool Scanning::LaserPowerDrop()
Plot of the laser charge distribution in time, the time values are calculating by using of the Movements_dt parameter.
bool Scanning::BeamSigma()
Plots the laser charge spread putting all the laser charges into a histogram
void Scanning::SwitchAxis(...)
Sets the number of scanning points, step and x0 for each axis.
void Scanning::CalculateCharges(...)
Calculates the charge profiles for different optical distances/voltages.
TGraph Scanning::NormedCharge(...)**
Calculates the normed charge profiles using the data from the photodetector.
void Scanning::FindEdges(...)
Looks for edges of the sensor for the Edge-TCT.
Double_t Scanning::Mu(Double_t E, Int_t Type)
Calculates the mobility value for holes or electrons as function of the electric field.
Double_t Scanning::BiSectionMethod(...)
Extracts the eletric field from the current, using the bisection method[7].

7 Conclusion

TCT signals were studied and processed for both edge- and top- scans. The operation of lasers was studied. The new PCB and mounts were tested and have shown the good results. The framework was developed for doing top- and edge- TCT measurements. Some functionality has to be added. A lot of ideas are going to be implemented soon.

References

[1] Marco Bomben et al, Nuclear Instruments and Methods in Physics Research Section A 712 (2013) 41-47.

[2] G.Kramberger et al, IEEE Transactions on Nuclear Science, vol. 57, no. 4, August 2010.

[3] http://particulars.si/downloads/Particulars-Procedures-LaserPulse.pdf.

[4] http://particulars.si/downloads/ParticularsProcedures-FocusFind.pdf

[5] Green MA, Keevers MJ. Optical properties of intrinsic silicon at 300 K. Progress in Photovoltaics: Research and Applications. 1995 ;3:189 - 192.

[6] Jiaguo Zhang DESY-THESIS-2013-018

[7] https://en.wikipedia.org/wiki/Bisection_method